ARTICLE

JAAS
www.rsc.org/jaas

LIBS limit of detection and plasma parameters of some elements in two different metallic matrices†

Marwa A. Ismail, Hisham Imam, Asmaa Elhassan, Walid T. Youniss and Mohamed A. Harith*

National Institute of Laser Enhanced Science (NILES), Cairo University, Giza, Egypt. E-mail: mharithm@egypt.com

Received 1st December 2003, Accepted 13th February 2004
First published as an Advance Article on the web 5th March 2004

In the present work a detailed study has been performed on the effect of the matrix on the limit of detection (LOD) and the plasma parameters of the laser induced breakdown spectroscopy (LIBS) technique. The LOD of magnesium, silicon, manganese and copper as minor elements was evaluated in aluminium standard sample alloys compared to the values of the LOD of the same elements in standard steel alloys. The effect of changing the matrix on the laser induced plasma plume parameters, namely the plasma temperature T_e and the electron density N_e, has been also studied. Calibrations were achieved for the four elements with linear regression coefficients between 98–99% on average. According to the obtained results Mn and Cu have the lowest LOD in the steel alloy matrix, while Mg has much lower LOD in the aluminium alloy matrix. These results may be interpreted in view of the compatibility of the physical properties of the elements existing in the same matrix. Approximately similar electronic structure and values of melting point, density, atomic weight, *etc.*, may facilitate better conditions for energy transfer within the matrix. From the application view point, it is possible for LIBS in the on-line industrial process control to follow up only a single element (that with the lowest LOD in such matrix) as a marker for the correct alloying in metals and mixing in pharmaceuticals.

Introduction

LIBS, as an elemental analytical technique, has been extended during the past two decades over a very wide range of analytical applications.[1] Simultaneous multi-element analysis of metals,[2] liquids,[3] biological and environmental samples[4] are among such numerous useful applications. However, one of the unsolved problems related to LIBS analysis is its sensitivity to the matrix effect and its influence on quantifying the analytical results. The matrix effect is generally defined as the strong dependence of the obtained atomic emission spectra on slight variation of the composition of the target in which the element of interest is embedded. Understanding the matrix effect is important to maximize LIBS analytical performance and to determine the technique limitations. The physical properties of the target, such as absorptivity, grain size, surface roughness, and thermal conductivity are among the main reasons for the matrix effect. In addition, plasma formation dynamics, sample ablation and associated processes are highly non-linear and not fully understood and may also play an important role as reasons for the matrix effect. Previously published works studied the matrix effect under different experimental conditions to specify causes and find out the methods of correction.[5–8]

Bulatov *et al.*[5] and Krasniker *et al.*[6] concluded that the matrix effect can be characterized by the amount of energy coupled into the plasma, which can be measured by following up the propagation velocity of the shock waves involved during the plasma formation growth. They suggested that the matrix effects are due to the higher emission from easily ionized elements existing in the matrix, which contribute to the first stages of plasma formation. They also studied the matrix influence on the electron temperature and electron number density.

Eppler *et al.*[7] exploited LIBS to investigate the effect of chemical speciation and matrix composition on Pb and Ba measurements in soil and sand matrices. Also, the ratios of the analyte signal to the signal from another element in the sample, at a fixed concentration (internal standard), was investigated. They stated that the trends of analyte emission intensities with speciation may be related to the physical properties of the compound (enthalpy of formation, enthalpy of vaporization, Gibbs free energy, entropy, enthalpy of fusion, heat capacity and molar volume). So they compared the internally standardized values of Pb and Ba from different compounds with some of the physical properties of the compounds.

Borisov *et al.*[9] and Margetic *et al.*[10] studied the effect of the laser pulse length on the Cu–Zn binary alloys. They found that, as the laser pulse duration decreases (pico- and femto-second), there is a non-linearity relation between the emission intensities of the spectral lines and the concentration of the corresponding analyte in the analyzed sample. This behavior is mainly due to the changes in the mass ablation rate.

In the present work the effect of the matrix on the LIBS limit of detection (LOD) of four elements (Mg, Si, Mn, and Cu) in two different matrices, aluminium and steel standard alloys, has been studied under same experimental conditions. A detailed investigation of the plasma parameters of the two alloys is presented and correlated to the matrix effect too.

Methodology

A typical LIBS experimental setup, described in detail elsewhere,[11] is used throughout the present investigations. Laser induced plasma was produced by focusing 70 mJ of Nd:YAG laser pulses (Surelite I, Continuum, USA) at 1064 nm with 7 ns duration on Al and steel alloy samples. The laser pulses were suitably focused on the sample in order to generate plasma. A fused-silica optical fiber (600 μm diameter) mounted on a micro *xyz*-translation stage is used to collect the emission light from the plasma plume and feed it to the echelle spectrometer.[12] The acquisition of the ICCD was delayed by 1.5 μs after the laser pulse was fired. However, to avoid

† Presented at the Second Euro-Mediterranean Symposium on Laser Induced Breakdown Spectroscopy, Hersonissos, Crete, Greece, September 30th–October 3rd, 2003.

DOI: 10.1039/b315588a

Table 1 The percentage elemental composition of the standard reference aluminium alloys

Sample No.	Mg (%)	Si (%)	Cu (%)	Mn (%)
1200 AG	0.016	0.17	0.017	0.025
3003 AG	0.015	0.26	0.12	1.09
6061 AJ	1.07	0.7	0.33	0.07
6111 AE	0.77	0.6	0.75	0.2
8006 AE	0.0041	0.25	0.049	0.53
356.2 AH	0.42	7.2	0.081	0.034

saturation of the detector, the integration time was limited to 1 μs. Such values of delay time and gate width are obtained after optimization procedures which will be mentioned later. The echelle spectrometer (Mechelle 7500, Multichannel Instruments, Sweden) has a focal length of 17 cm with *f*-number of 5.2. It provides a constant spectral resolution of 7500 corresponding to 4 pixels FWHM, over a wavelength range 200–1000 nm, displayable in a single spectrum. Gateable ICCD camera, (DiCAM-Pro-PCO computer optics, Germany), with a high-resolution sensor with 1280 × 1024 pixels (9 × 9 mm^2) coupled to the spectrometer, was used for the detection of the dispersed light. The 25 mm microchannel plate is from the DiCAM with a UV-enhanced photocathode. The overall linear dispersion of the Mechelle spectrometer–camera system ranges from 0.0078 (at 200 nm) to 0.038 nm $pixel^{-1}$ (at 1000 nm). The ICCD camera control was performed *via* special multichannel instrument software. Spectra display, processing and analysis were done using 2D- and 3D-Gram/32 software programs (National Instruments, USA). In addition to the atomic database used by the mentioned software, spectral lines identification was checked by electronically published database.[13]

The analyzed samples are certified standard aluminium and steel alloys. The common trace elements in both of the aluminium and steel samples are Mg, Si, Mn, and Cu. The elemental composition of the samples under study is listed in Table 1 for the aluminium alloys and in Table 2 for the steel alloys.

All measurements have been performed at atmospheric air pressure. As mentioned in pervious papers[14–16] the samples need to be exposed to a certain number of preparation laser shots before performing the measurement in order to ensure that the surface of the target is representative to the bulk composition and also to eliminate any surface impurities. The collected spectra are the average of 5 shots at 5 different target positions, *i.e.* the average of 25 accumulated spectra. This improves the statistical fluctuations and compensate for any expected target inhomogeneity.

LIBS spectra have been obtained for both sample types under similar experimental conditions (laser wavelength, energy/pulse, repetition rate, delay time, gate width *etc.*). Such experimental conditions have been optimized in order to reduce the background signal and increase the signal to noise ratio (S/N). For quantitative analysis using LIBS technique the measurements should be time resolved in order to get rid of the overwhelming high intensity continuum emission at the early time of the plasma formation.[17,18] So, in order to obtain the best detection limit the delay time is optimized using both ionic and neutral lines normalized to the background. Fig. 1a and b show that, the maximum emission of both neutral and ionic lines, occur after a delay of 1.5 μs.

Table 2 The percentage elemental composition of the standard reference steel alloys

Sample No.	Mg (%)	Si (%)	Cu (%)	Mn (%)
1261 a AISI 4340 steel	0.00018	0.228	0.042	0.67
1262 a AISI 94B17 modified	0.000062	0.4	0.51	1.05
1263 a Cr-V steel modified	0.00049	0.74	0.09	1.5
1264 a high carbon steel	0.00015	0.067	0.25	0.25
1265 a electrolytic iron		0.008	0.0058	0.0057

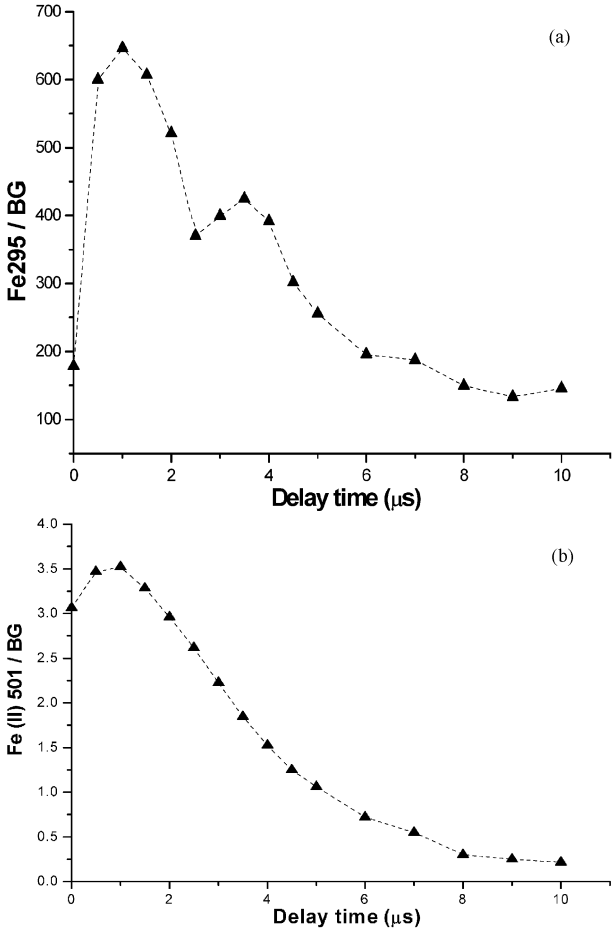

Fig. 1 (a) Delay time optimization of neutral lines. (b) Delay time optimization of ionic lines.

Results and discussion

Spectra

Figs. 2a and b show typical LIBS spectra for aluminium and steel alloys. Each of these spectra is, as mentioned before, the average of a 25 single shot spectra. It is clear from these spectra that the rich transitions in the iron atoms make the steel alloy spectrum much more crowded than that of the aluminium alloy. This, of course, makes the analysis of the steel spectra much more tedious, and needs a very high-resolution spectroscopic system.

Calibration curves

The availability of certified standard samples makes it easy to construct calibration curves for each of the elements included in each alloy. Internal standardization method has been exploited to avoid any unwanted experimental fluctuations.[19] The ratio of the line intensity of trace element to the emission line of the internal standard is measured and plotted as a function of the known concentration ratios of the reference samples. The proper emission line of the internal standard has been chosen by comparing different calibration curves of the same element obtained using different internal standards and different emission lines. The element and line giving the best linear relation (the highest value of the correlation coefficient *R*) are chosen as internal standards. The performed optimization in case of the minor elements in the aluminium alloy (Mg, Si, Mn and Cu), revealed that the best internal standard is the

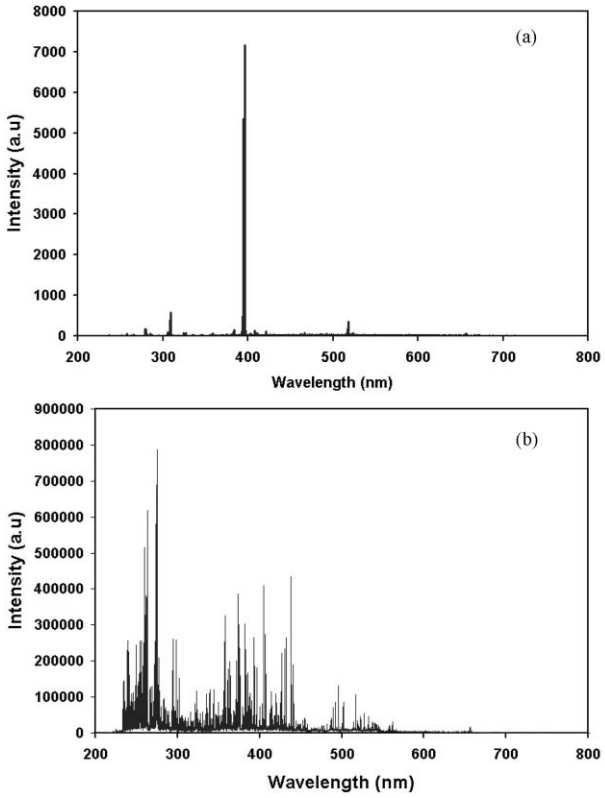

Fig. 2 (a) Typical LIBS spectrum for aluminium alloy target. (b) Typical LIBS spectrum for steel alloy target.

Al atomic line at 305 nm. This is in agreement with previously published data, recommending the use of a major element in the matrix as an internal standard.[11] On the other hand, in case of the steel alloy the optimum internal standard line was the iron atomic line at 375.82 nm for the same minor elements. Although other authors have used other internal standard iron lines and the well known strong line of carbon at 247.8 nm,[18,20] the iron 375.82 nm line represented a better choice in the present case. This well resolved strong iron line is nearly centered in the spectral window including the analyzed lines. In addition, its upper energy level is very close to that of the analyzed lines as well, thus reducing the possibility of temperature fluctuations affecting the ratios.

Calibration curves and limit of detection

The wavelengths of the spectral lines used throughout the analysis were Mg I (285.21 nm), Si I (288.15 nm), Mn I (403.07 nm), and Cu I (324.75 nm): the spectroscopic parameters of these lines are taken from ref. 31. The corresponding normalized calibration curves are given in Figs. 3–6, for aluminium and steel. Mg (285.21 nm), Mn (403.07 nm), and Cu (324.75 nm) are resonance lines, *i.e.* the lower level of the transition is the ground state. Normally we have to avoid such lines in the quantitative analysis since they are subjective of high self absorption. Since the number density of the atomic species of Mg, Mn, and Cu in the plasma plume is low due to their low concentration in the target material, self absorption effect may be neglected within the experimental uncertainty although of the slight departure from linearity in case of the Mg calibration curve in steel. So, these lines are good candidates for a lower limit of detection due to its strength compared with other atomic emission lines. This is, in fact, in agreement with the observations of Sabsabi and Cielo,[17] Lazic *et al.*,[21] and Telle *et al.*[22]

Generally, Mn and Cu calibration curves show good linearity over broad range of concentrations in steel samples, while Mg is the optimum in case of aluminium samples.

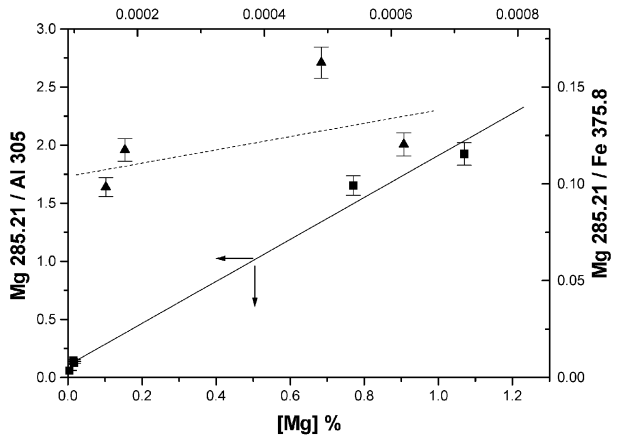

Fig. 3 Calibration curves of Mg in aluminium alloy (squares) and in steel alloy (triangles).

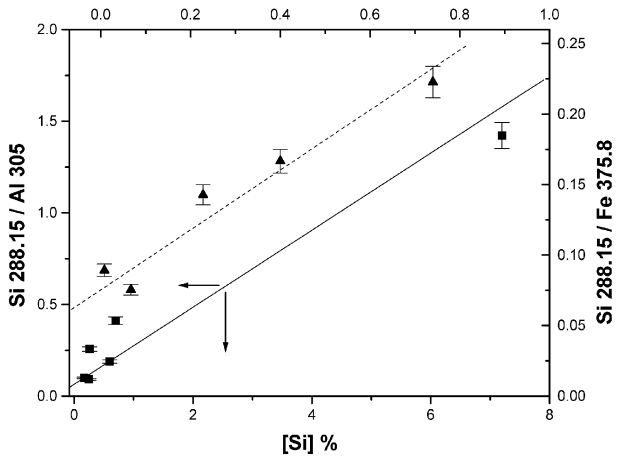

Fig. 4 Calibration curves of Si in aluminium alloy (squares) and in steel alloy (triangles).

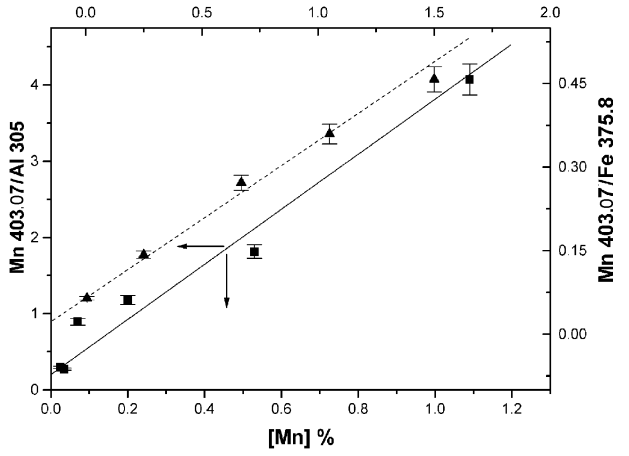

Fig. 5 Calibration curves of Mn in aluminium alloy (squares) and in steel alloy (triangles).

Calibration curves of the elements in the aluminium matrix pass nearly through the origin within the experimental uncertainty; however, the calibration curves of the same elements in steel matrix did not pass through the origin. This phenomenon can be attributed to a systematic over-estimation of the intensity of the lines in steel matrix having such line rich spectrum.

The limit of detection (LOD) calculation is based on the $3\sigma_B$-IUPAC definition.[23]

$$\mathrm{LOD} = \frac{3\sigma_B}{S} \quad (1)$$

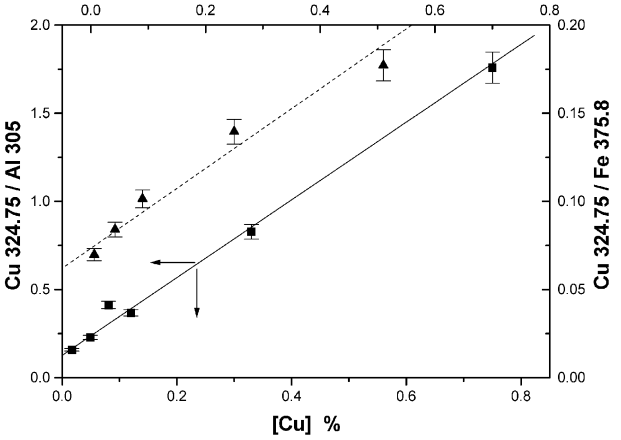

Fig. 6 Calibration curves of Cu in aluminium alloy (squares) and in steel alloy (triangles).

where, σ_B is the standard deviation of the background, and S is the slope of the calibration line. The limit of detection of each of the minor elements in aluminium and steel alloys calculated by eqn. (1), the relative standard deviation (RSD%), and correlation coefficient (R) are listed in Tables 3 and 4.

Mn and Cu (in steel matrix) have good LOD, best correlation coefficient and lower RSD%, where lower RSD% indicates better reproducibility and sample homogeneity. However, the LOD of these two elements in the aluminium matrix is not as good as their LOD values in the steel matrix. Silicon has poor LOD in aluminium matrix while its value in steel matrix is very good. Contrary to the other three elements under investigation, Mg has a better LOD and correlation coefficient in aluminium than in steel matrix, taking into consideration the slight self absorption showing up in its calibration curves.

These observations can be explained considering the physical properties of the elements under study relative to the major element of the matrix, since the matrix effect is the change in the plasma composition produced by the physical and chemical properties of the target. Some of these physical constants are listed in Table 5.

Since Mn, and Cu have some physical properties (atomic weight, boiling point, melting point, specific heat, density, and ionization potential) which are very close to that of Fe (major element of steel alloy) and far from those of Al (major element of aluminium alloy), this may have some effect on the obtained values of the LOD of the studied elements in both matrices mainly due to the ease of the energy transfer between the elements within each matrix. The same effect can be also noticed in case of Mg and Si results.

Table 3 Limit of detection (LOD), relative standard deviation (RSD%), and correlation coefficient (R^2) values for the elements under study in aluminium alloy

Wavelength	LOD (ppm)	RSD%	R^2
Mg (285 nm)	28.16	3.1	0.99
Si (288 nm)	283.9	9.12	0.98
Mn (403 nm)	15.28	3.17	0.98
Cu (324 nm)	23.8	5.05	0.99

Table 4 Limit of detection (LOD), relative standard deviation (RSD%), and correlation coefficient (R^2) values for the elements under study in steel alloy

Wavelength	LOD (ppm)	RSD%	R^2
Mg (285 nm)	76.78	4.12	0.56
Si (288 nm)	6.64	1.46	0.97
Mn (403 nm)	4.99	3.41	0.99
Cu (324 nm)	6.31	6.31	0.98

Plasma parameters

The matrix effect may affect the plasma conditions (plasma temperature and electron density), where the plasma temperature is an important parameter for determining the elemental composition. The spectral line intensity is essential to infer the plasma temperature, where the allowed spectral line transition intensity of certain element can be represented by Boltzmann equation as:

$$I = FC_s \frac{A_{ki} g_k}{U_s(T)} \exp\left[-\frac{E_k}{kT}\right] \quad (2)$$

where A_{ki} is the transition probability, g_k is the statistical weight for the upper level, E_k is the excited level energy, T is the temperature, k is the Boltzmann constant, $U_s(T)$ is the partition function of the species, F is an experimental factor and C_s is the species concentration. Reformulating eqn. (2) gives:

$$\ln \frac{I}{A_{ki} g_k} = -\frac{1}{kT} E_k + \ln \frac{C_s F}{U_s(T)} \quad (3)$$

By plotting the left hand side of eqn. (3) *vs.* the excited level energy E_k, the plasma temperature can be obtained from the slope of obtained straight line.

There are several factors to be taken into consideration for reliable results,[24] under these requirements eight atomic spectral lines of iron were used to infer the temperature in aluminium and steel samples. These lines are (in nm): 370.55, 371.99, 372.25, 373.48, 373.71, 374.56, 375.82 and 376.38. Their values of degeneracy, transition probability and other constants are listed in ref. 25.

A typical plot of eqn. (3) is shown in Fig. 7, where the data were fitted with least-square approximation. The slope of the curve yields a temperature of 8400 K in aluminium alloy and 11000 K in steel alloy. This difference in the plasma temperature of the two alloys can be attributed to the difference in the ionization potential of the elements Fe and Al, see Table 5. Under the same experimental conditions the higher the ionization potential of the major element of the alloy, the higher is the plasma temperature, which is the same situation of Fe and Al ionization potentials and the corresponding plasma temperatures.

Electron density

Pressure broadening, Doppler broadening and Stark broadening are mechanisms involved in the spectral line broadening

Table 5 Physical constants of different elements in the investigated samples

Element	Atomic number	Atomic weight/u	Boiling point/K	Melting point/K	Specific heat/J gm^{-1} K^{-1}	Ionization potential/eV
Mg	12	24.305	1363	922	1.02	7.64
Al	13	26.98	2740	933.52	0.9	5.98
Si	14	28.08	2628	1683	0.71	8.15
Mn	25	54.93	2235	1517	0.48	7.43
Fe	26	55.84	3023	1809	0.444	7.87
Cu	29	63.54	2836	1356.6	0.38	7.72

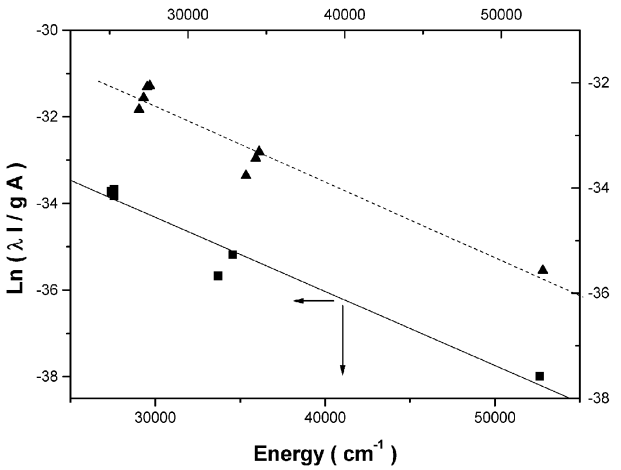

Fig. 7 Typical Boltzmann plots for aluminium alloy (squares) and for steel alloy (triangles).

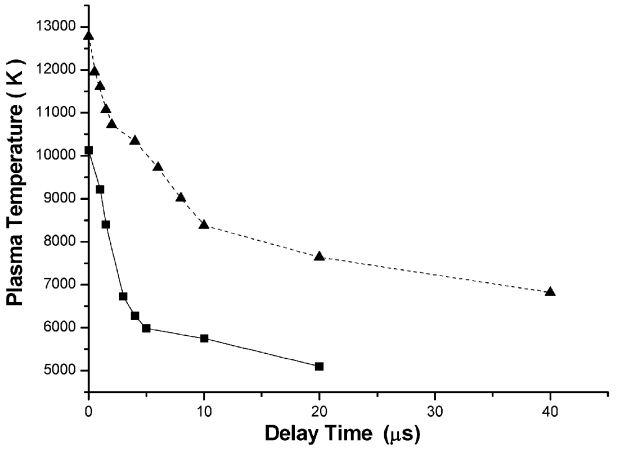

Fig. 8 Temporal behavior of plasma temperature of aluminium alloy (squares) and for steel alloy (triangles).

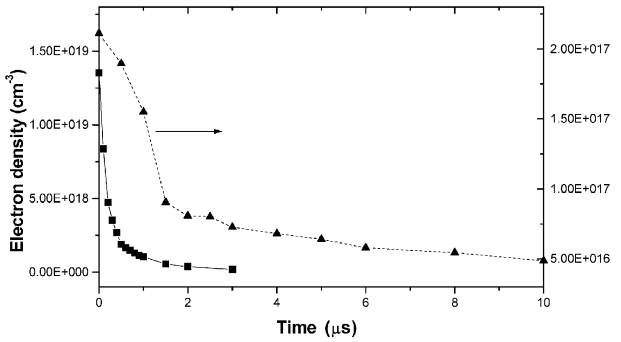

Fig. 9 Temporal behavior of plasma density for aluminium alloy (squares), and for steel alloy (triangles).

in laser-induced plasma. According to Sabsabi and Cielo,[17] and Milán and Laserna,[26] Stark broadening mechanism dominates in the plasma temperature range of the present experiment. The profile of Stark broadened lines is well described by a Lorentz function. Since the instrumental line-broadening exhibits a Lorentzian shape, then the stark line width $\Delta\lambda_{true}$ can be extracted from the measured line width $\Delta\lambda_{observed}$ by subtracting the instrumental line broadening $\Delta\lambda_{instrument}$:

$$\Delta\lambda_{true} = \Delta\lambda_{observed} - \Delta\lambda_{instrument} \quad (4)$$

In our case $\Delta\lambda_{instrument}$ was 0.05 nm (determined by measuring the FWHM of the Hg lines emitted by a standard low presser Hg lamp).

The width of stark broadened spectral line depends on the electron density (N_e). For the linear Stark effect the electron density and the line width are related by the simple formula

$$N_e = C(N_e, T)\Delta\lambda^{3/2}_{FWHM} \quad (5)$$

The parameter $C(N_e, T)$ determines the relative contribution of the electron collision on the electrostatic fields, and it depends weakly on N_e and T.

For a non-H like line, the electron density (in cm^{-3}) can be determined from the line width as:

$$N_e \approx \left[\frac{\Delta\lambda_{FWHM}}{2w}\right] \times 10^{16} \quad (6)$$

The parameter w is the electron impact value, and it can be found in a well documented table.[27] This was in case of Al in aluminium alloy, but in case of Fe in steel alloy, the stark broadening parameter of this line is reported previously with 4% uncertainty.[28]

In this way the electron density for aluminium alloy is 5.45×10^{17} cm^{-3} and its value for the steel alloy is 9.047×10^{16} cm^{-3}. These results are logical physically, in view of the values of the ionization potential of Al and Fe because, the lower the ionization potential (IP) of the major element, the higher is the electron density of the plasma.

The temporal evolution of the plasma temperature, for aluminium and steel alloys, shown in Fig. 8, depicts fast cooling down of the plasma followed by slow dynamics at later times.

The temporal behavior of the electron density, shown in Fig. 9 for aluminium and steel alloys, show the effect of collisional processes by the high value of the electron density at the early time of the plasma evolution, while the recombination processes are very clear at longer delay time.

Finally, by knowing the electron density and the plasma temperature we can determine whether the local thermodynamic equilibrium (LTE) assumption is valid by applying the criterion given by McWhirter.[29]

The lower limit for the electron density at which the plasma will be in LTE is given by:

$$N_e(cm^{-3}) \geqslant 1.6 \times 10^{12}[T(K)]^{1/2}[\Delta E(eV)]^3 \quad (7)$$

ΔE is the largest energy transition for which the condition holds and T is the excitation temperature.[17,30]

In the present case $\Delta E = 4.34$ eV for Mg (see ref. 31). The electron density lower limit value given by eqn. (7) is 12×10^{15} cm^{-3} for aluminium plasma, and is 13.7×10^{15} cm^{-3} in case of steel plasma, where the experimentally calculated densities are greater than these values, which is consistent with the assumption that the LTE prevailing in the plasma.

Conclusion

The present investigations show that the differences in the LIBS limit of detection of the same element in different matrices can be correlated with the compatibility of the physical properties of the elements existing in the same matrix. Approximately similar electronic structures may facilitate better conditions for energy transfer within the matrix and consequently raising the technique sensitivity. The target physical properties play an important role in the obtained values of the laser induced plasma temperature T_e and electron density N_e. These, in turn, affect the spectral characteristics of each element in the same matrix.

The obtained results indicate that it is possible to improve the exploitation of LIBS in the on-line industrial process control, by following up only a single element (that with the

lowest LOD in such matrix) as a marker for the correct alloying in metals and mixing in pharmaceuticals.

Acknowledgements

The authors gratefully appreciate the help of Dr. Hussain Abd Elmoniem in the early stages of the measurements.

References

1 *Laser Induced Plasmas and Applications*, ed. L. J. Radziemski and D. A. Cremers, Marcel Decker, Inc, New York, 1989.
2 R. Noll, H. Bette, A. Brysch, M. Kraushaar, I. Mönch, L. Peter and V. Sturm, *Spectrochim. Acta, Part B*, 2001, **56**, 637.
3 B. Charfi and M. A. Harith, *Spectrochim. Acta, Part B*, 2002, **57**, 1141.
4 R. T. Wainner, R. S. Harmon, A. W. Miziolek, K. L. Mcnesby and P. D. French, *Spectrochim. Acta, Part B*, 2001, **56**, 777.
5 V. Bulatov, R. Krasniker and I. Schechter, *Anal. Chem.*, 1998, **70**, 5302.
6 R. Krasniker, V. Bulatov and I. Schechter, *Spectrochim. Acta, Part B*, 2001, **56**, 609.
7 A. S. Eppler, D. A. Cremers, D. D. Hickmott, M. J. Ferris and A. C. Koskelo, *Appl. Spectrosc.*, 1996, **50**, 1175.
8 C. Chaleard, P. Mauchien, N. Andre, J. Uebbing, J. L. Lacour and C. Geertsen, *J. Anal. At. Spectrom.*, 1997, **12**, 183.
9 O. V. Borisov, X. L. Mao, A. Fernandez, M. Caetano and R. E. Russo, *Spectrochim. Acta, Part B*, 1999, **54**, 1351.
10 V. Margetic, K. Niemax and R. Hergenröder, *Spectrochim. Acta, Part B*, 2001, **56**, 1003.
11 M. Sabsabi, V. Detalle, M. A. Harith, W. Tawfik and H. Imam, *Appl. Opt.*, 2003, **42**, 6094.
12 J. W. Olesik, *Spectroscopy*, 1999, **14**, 27.
13 NIST electronic database, http://physlab.nist.gov/physRefData/contents-atomic.html.
14 J. A. Aguilera, C. Aragón and J. Campos, *Appl. Spectrosc.*, 1992, **46**, 1382.
15 S. Palanco and J. J. Laserna, *J. Anal. At. Spectrom.*, 2000, **15**, 1321.
16 L. St-Onge, M. Sabsabi and P. Cielo, *J. Anal. At. Spectrom.*, 1997, **12**, 997.
17 M. Sabsabi and P. Cielo, *Appl. Spectrosc.*, 1995, **49**, 499.
18 Q. Sun, M. Tran, B. W. Smith and J. D. Winefordner, *Anal. Chim. Acta*, 2000, **413**, 187.
19 Y. Yoon, T. Kim, M. Yang, K. Lee and G. Lee, *Microchem. J.*, 2001, **68**, 251.
20 M. Hemmelin, R. Meilland, H. Falk, P. Wintjens and L. Paulard, *Spectrochim. Acta, Part B*, 2001, **56**, 661.
21 V. Lazic, R. Barbini, F. Colao, R. Fantoni and A. Palucci, *Spectrochim. Acta, Part B*, 2001, **56**, 807.
22 H. H. Telle, D. C. S. Beddows, G. W. Morris and O. Samek, *Spectrochim. Acta, Part B*, 2001, **56**, 947.
23 J. D. Ingle and S. R. Crouch, in *Spectrochemical Analysis*, ed. K. M. Lafferty, Prentice Hall, New Jersey, 1988.
24 C. F. Su, S. Feng, J. P. Singh, F. Yueh, J. T. Rigsby III, D. L. Monts and R. L. Cook, *Glass Technol.*, 2000, **41**, 16.
25 J. R. Fuhr, G. A. Martin, W. L. Wiese and S. M. Younger, in *Spectroscopic Data for Iron, ORNL-6089/V4*, ed. W. L. Wiese, Oak Ridge National Laboratory, Oak Ridge, Tennessee, 1985.
26 M. Milán and J. J. Laserna, *Spectrochim. Acta, Part B*, 2001, **56**, 275.
27 H. R. Griem, *Plasma Spectroscopy*, McGraw-Hill, New York, 1964.
28 S. Freudenstein and J. Cooper, *Astron. Astrophys.*, 1979, **71**, 283.
29 R. W. P. McWhirter, in *Plasma Diagnostic Techniques*, ed. R. H. Huddlestone and S. L. Leonard, Academic Press, New York, 1965, ch. 5, p. 206.
30 O. Samek, D. C. S. Beddows, J. Kaiser, S. V. Kukhlevsky, M. Liška, H. H. Telle and J. Young, *Opt. Eng.*, 2000, **39**, 2248.
31 W. L. Wiese, M. W. Smith and B. M. Miles, *Atomic Transition Probabilities, Vol. II, Sodium through Calcium Critical Data Compilation, National Standard Reference Data System-NBS22*, US Government Printing Office, Washington, DC, 1969; J. Reader, C. H. Corliss, W. L. Wiese and O. A. Martin, *Wavelength and Transition Probabilities for Atoms and Atomic Ions, National Standard Reference Data System-NBS 68*, US Government Printing Office, Washington, DC, 1980.